Validation of a transient zonal model to predict the detailed indoor thermal environment: case of electric radiators and wood stoves

L. Georges[1,*], M. Thalfeldt[1], Ø. Skreiberg[2] and W. Fornari[3]

[1]*Norwegian University of Science and Technology (NTNU), Trondheim, Norway*
[2]*SINTEF Energy Research, Trondheim, Norway*
[3]*EQUA Simulation AB, Solna, Sweden*
**Corresponding author: laurent.georges@ntnu.no*

Abstract

In building performance simulation (BPS), zonal models are intermediate models between standard models assuming perfectly-mixed room air and Computational Fluid Dynamics (CFD): they aim to predict the air temperature and velocity fields as well as the pollutant distribution inside a room using a computational time significantly lower than using CFD. The article aims at validating a transient zonal model that is currently implemented in the commercial BPS tool, IDA ICE. In theory, this one-dimensional model can address a large variety of airflows and requires almost no *a priori* knowledge of the flow to be computed. The model is validated against measurements in a laboratory heated by either electric radiators or an electric stove designed to mimic surface temperatures of real stoves. Unlike radiators, the case of stoves has never been addressed in the literature and is challenging due to the strong thermal coupling between the room air and walls. Heat emitters have been placed either in the middle of the room or along walls. The zonal model remarkably well predicts the time evolution of the air temperature stratification in the room for all test cases. For a heat emitter in a central position, the wall surface temperatures are predicted correctly. Nevertheless, for a heat emitter along walls, these walls cannot be considered isothermal anymore, an assumption found in most BPS tools. The paper suggests that an automatized method to divide walls in the vicinity of heat emitters is necessary for a reliable prediction of the wall surface temperatures.

Nomenclature

T_i	*air temperature in layer (i)*
$\overline{T}_{air}$	*volume-averaged air temperature in the room*
T_∞	*air temperature of the environment around the plume*
T_w	*surface temperature of the wall*
T_{mrt}	*mean radiant temperature at the location of a black globe*
T_{op}	*operative temperature at the location of a black globe*
$T_{e,i}$	*average air temperature of wall current (e) at the level of layer (i)*
$T_{flow,i\to e}$	*average air temperature of wall current (e) resulting from air entering from layer (i)*
T_s	*surface temperature of the heat emitter*
$\dot{m}_{lay,i}$	*mass flow from layer (i) to layer (i+1)*
$\dot{m}_{flow,i}$	*net mass flow from all the flow elements to layer (i)*
$\dot{m}_{flow,j\to i}$	*mass flow from flow element (j) to layer (i)*

$\dot{m}_{flow,i\to j}$	*mass flow from layer (i) entrained in flow element (j)*
$\dot{m}_{flow,i\to e}$	*mass flow from layer (i) entrained in wall current (e)*
$\dot{m}_{e,i}$	*total mass flow in the wall current (e) at the height of layer (i)*
$\dot{m}_{de,i}$	*mass flow from layer (i+1) to layer (i) transported by the wall current (e)*
$\dot{Q}_{flow,i}$	*net energy input to layer (i) from all the flow elements*
$\dot{Q}_{flow,j\to i}$	*heat flux from element (j) to layer (i)*
$\dot{Q}_{flow,i\to j}$	*heat flux from layer (i) to element (j)*
$\dot{Q}_{cond,i}$	*heat flux from layer (i) to layer (i+1) generated by thermal conduction*
$\dot{Q}_{trans,i}$	*heat transported from layer (i) to layer (i+1)*
P_c	*power emitted in form of convection*
P_r	*power emitted in form of thermal radiation*
P_{tot}	*total power emitted in form of convection and thermal radiation*
q_p	*plume volume flow*
m	*plume momentum*
B	*plume buoyancy flux*
ρ	*air density*
$C_{p,eff}$	*effective specific heat of layer (i)*
$C_{p,air}$	*specific heat of air*
$h_{c,air}$	*convection coefficient for a given wall*
k_{eff}	*effective thermal conductivity of air*
k_{air}	*thermal conductivity of air*
β	*coefficient of thermal expansion of air*
σ	*Stefan-Boltzmann constant*
ε	*emissivity of a surface*
α	*entrainment factor of the plume*
A_i	*area of the horizontal surface separating layers (i+1) and (i)*
$A_{w,i}$	*area of the vertical surface connecting layer (i) and the wall*
V_i	*volume of air in layer (i)*
h_i	*height of layer (i)*
z	*axial direction of the plume (or vertical direction)*

1 Introduction

Different modelling approaches can be used to evaluate airflows and the spatial distribution of temperature and pollutants inside a room [1, 2]. Nevertheless, commercial building performance simulation (BPS) software assume that each building zone is well-mixed. It means that the temperature and concentration of pollutants (or humidity) is considered uniform in the entire air volume of the zone. In addition, air velocity is not computed. This modelling approach is here called the standard

room model. Many commercial BPS tools incorporate airflow networks that enable to compute airflow rates between well-mixed zones. Even though airflow networks proved to successfully address many important engineering and design problems, they are not developed to capture airflows inside rooms [3], while this information is paramount for a detailed assessment of thermal comfort and indoor air quality (IAQ). Computational Fluid Dynamics (CFD) enables to compute airflows inside a room [4] but suffers from major drawbacks when applied to building airflows, see e.g. [5, 6] regarding turbulence modelling. One main drawback is the computational time as hundred thousand to millions of grid points are required (as a function of the physics of the airflow to be computed, the numerical method and the turbulence modelling approach selected). Zonal models represent an intermediate approach between the standard room model and CFD. They aim to predict air movement, temperature and pollutant distributions in a room with extremely less computational time than CFD. Yearly simulations could even be considered. A large variety of zonal models have been proposed in the past with different modelling strategies. Although different, they all proposed to split the room in many nodes where the air temperature and concentration of pollutants are computed. In addition, many zonal models also enable to compute the air velocity inside the room (but this is not systematically done by all zonal models). An extensive review of the existing zonal models is beyond the scope of the article and can be found in references [7-9]. A common way to classify zonal models is to distinguish between pressurized and non-pressurized zonal models. In pressurized models, such as the POMA or VEPZO models [10-12], the mass flow between two neighbouring air nodes is evaluated based on their respective static pressure. Pressurized models make the generalization to three-dimensional (3D) models more straightforward. Non-pressurized models do not evaluate the pressure in each air node. Finally, as an alternative to zonal models, some intermediate methods rely on an approximate resolution of the Navier-Stokes equations. It can be done using CFD on a coarse grid [13] or using a simplified numerical method, such as the Fast Fluid Dynamics (FFD) [14, 15].

To date, zonal models are not implemented in commercial BPS software but this situation may change. IDA ICE is a building simulation software developed by the company EQUA located in Sweden and is widely used by research and industry, for instance in Scandinavia. EQUA has recently proposed a new zonal model [16] that is currently under implementation in IDA ICE. For the room air, this non-pressurized model is similar to the zonal model of Togari [17-20] already formulated in the early nineties. Regarding the longwave radiation between walls, heat exchange is computed using the radiosity method where view factors are evaluated numerically. The view factor algorithm enables to account for non-convex geometries, such as L-shaped rooms or obstacles between walls. This new zonal model has been proposed by EQUA because of its ability to cover a large spectrum of airflows (e.g. displacement ventilation, heat emitters). In addition, it requires limited input data and (almost) no *a priori* knowledge of the airflow to be solved. These are important criteria for the implementation in a commercial BPS tool. In this context, the range of validity and robustness of the model should be properly evaluated. In their original paper [16], EQUA tested the performance of their zonal model in one natural convection and one displacement ventilation benchmark. Results were promising but extended validations were still required.

This article proposes to validate and document the performance of the new zonal model in the context of heat emission systems, namely electric radiators and wood stoves. The case of electric radiators has been already addressed in the past by other zonal models that were able to successfully predict the thermal stratification, see e.g. [21-23]. Nevertheless, wood stoves have never been considered. This is a challenging test case due to the characteristics of the batch combustion process in wood stoves. The heat emitted to the room has an instantaneous power significantly larger than the room heat losses so the room thermal mass plays a major role to limit indoor temperature [24, 25]. In addition, the stove has a transient heat release profile to the room. Consequently, the zonal model should be able to

capture the strong thermal coupling between the heat source, room surfaces and the air, as well as transient behaviour. Previous investigations using field measurements [26] have shown that thermal stratification is non negligible when using wood stoves and can impair thermal comfort [27]. The standard room model proved to predict the operative temperature relatively well but is, by definition, unable to evaluate thermal stratification. Regarding longwave radiation, the stove geometry is introduced inside the virtual geometrical room model in the new IDA ICE model. A wood stove is thus an obstacle between walls so that view factors need to be evaluated numerically.

In order to validate the zonal model, experiments were performed in a test cell located in Trondheim (Norway). The cell was heated using an electric radiator and a convector while an electric stove has been used (instead of a real one). The surface temperatures of the electric stove are controlled by adapting the heat release of electric resistances so that realistic transient surface temperatures of wood stoves can be imposed. By using an electric stove, it is also possible to accurately measure the heat emitted to the room, an important input to validate the model.

The paper is organized as follows. In Section 2, the zonal model and its implementation are first introduced. Section 3 describes the experimental setup. Results are presented in Section 4 and discussed in Section 5. Conclusions are given in Section 6.

2 Zonal model

2.1 Description

The most general formulation of the zonal model can be found in [16]. For the sake of the simplicity, only the part of this zonal model which is physically active for our test case will be introduced in the paper. In fact, models for boundary layers along walls and the plume of heat emitters will be explained, while equations for non-isothermal attached and free jets will not be covered. The zonal model divides the room in several horizontal layers with uniform air temperature per layer and negligible velocity. Therefore, this leads to a one-dimensional (1D) model that enables to account for temperature stratification. The time derivative of the air temperature in each layer is computed based on the conservation of energy in an open system. An important input to this conservation equation is the mass flow exchanged between layers. This quantity is established using the conservation of mass and analytical models for the main flow phenomena in the room, called flow elements. In our test, dominated by natural convection, the main flow element is the thermal plume generated by heat emitters. The entrainment of the plume pumps colder air inside the plume from the lower layers of the room. The warm air from the plume is then injected into the higher layers of the room. Colder walls pump warm air from the higher air layers into the so-called wall currents. This air is injected back from the wall currents into the bulk of the flow in the lower layers of the room. This balance of mass flows between the plume and boundary layer effects is at the origin of the thermal stratification. The overall principle is shown in Figure 1. For each layer (i), the conservation of mass can be expressed in the following way:

$$\dot{m}_{lay,i} = \dot{m}_{lay,i-1} + \dot{m}_{flow,i} \ , \tag{1}$$

$$\dot{m}_{flow,i} = \sum_{j=1}^{Ne} (\dot{m}_{flow,j\to i} - \dot{m}_{flow,i\to j}) \ , \tag{2}$$

where $\dot{m}_{lay,i}$ is the mass flow from layer (i) to layer (i+1), $\dot{m}_{flow,i}$ is the net mass flow from all the *Ne* flow elements to layer (i). A flow element (j) can either inject mass into ($\dot{m}_{flow,j\to i}$) or entrain mass from the layer (i), ($\dot{m}_{flow,i\to j}$).

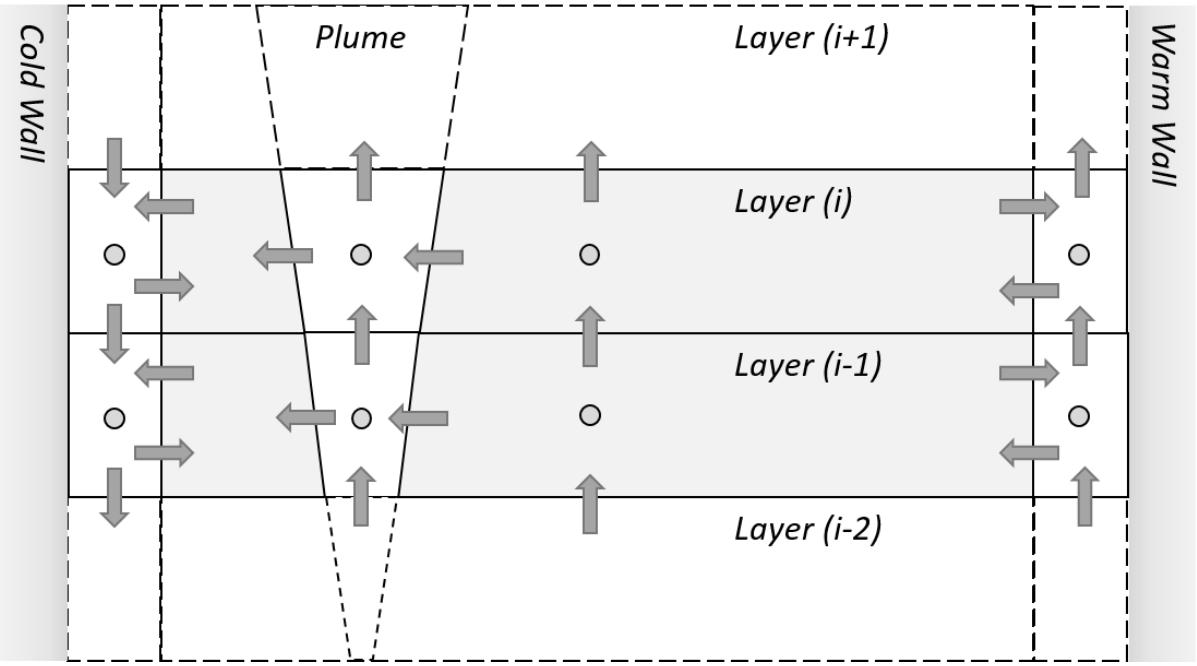

Figure 1. Sketch of a room discretized using horizontal layers and the main flow elements (i.e. wall currents and thermal plumes).

The conservation of energy is discretized in space using a finite volume method. It enables to evaluate the time derivative of the air temperature T_i in each layer:

$$\rho V_i C_{p,eff}\, dT_i/dt = (\dot{Q}_{cond,i} - \dot{Q}_{cond,i-1}) + (\dot{Q}_{trans,i} - \dot{Q}_{trans,i-1}) + \dot{Q}_{flow,i}\ , \tag{3}$$

where ρ is the air density, V_i is the air volume of layer (i) and $C_{p,eff}$ is the effective specific heat of layer (i) in [kJ/K.kg]. This quantity is higher than the specific heat of air ($C_{p,air}$) due to the presence of measurement devices or furniture. $\dot{Q}_{cond,i}$ is the heat flux from layer (i) to layer (i+1) generated by thermal conduction. This term is computed using:

$$\dot{Q}_{cond,i} = k_{eff} A_i (T_{i+1} - T_i)/((h_{i+1} + h_i)/2)\,, \tag{4}$$

where k_{eff} is the effective thermal conductivity of air (which may be higher than the physical thermal conductivity of air, k_{air}, due to turbulence mixing [20, 28]), A_i is the area of the horizontal surface separating layers (i+1) and (i) and h_i is the height of layer (i). The heat transported from layer (i) to layer (i+1) is computed using

$$\dot{Q}_{trans,i} = \max(\dot{m}_{lay,i}, 0) C_{p,air} T_i + \min(\dot{m}_{lay,i}, 0) C_{p,air} T_{i+1}\ . \tag{5}$$

The final term in Eq. (3) is net energy input to layer (i) from all the *Ne* flow elements, $\dot{Q}_{flow,i}$:

$$\dot{Q}_{flow,i} = \sum_{j=1}^{Ne} (\dot{Q}_{flow,j\to i} - \dot{Q}_{flow,i\to j}) \ , \tag{6}$$

where $\dot{Q}_{flow,j\to i}$ is the heat flux from element (j) to layer (i) and $\dot{Q}_{flow,i\to j}$ is the heat flux from layer (i) to element (j).

The zonal model is 1D and the velocity is assumed to be low in each layer. It belongs to the category of non-pressurized zonal models [8]. By computing pressure in each air node, pressurized models can typically discretize space in the horizontal direction as well, creating two or three-dimensional velocity fields. In this way, these pressurized models can evaluate flow recirculation or velocity in the occupancy zone. On the contrary, the present zonal model can only evaluate draught effects when the occupant is in direct contact with flow elements, not due to an overall flow movement in the room.

2.2 Wall boundary layers

To close this system of equations, a formula should be found for the heat and mass flows from and to the flow elements: $\dot{m}_{flow,j\to i}$, $\dot{m}_{flow,i\to j}$, $\dot{Q}_{flow,j\to i}$ and $\dot{Q}_{flow,i\to j}$.

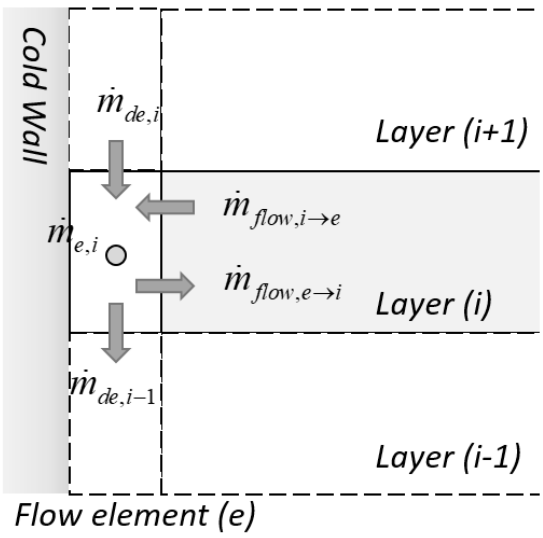

Figure 2. Sketch of the main flow variables in a wall current for the example case of a cold wall.

A sketch of the wall current (e) is shown in Figure 2 for the case of a cold wall. The positive heat flux $\dot{Q}_{flow,i\to e}$ from layer (i) to the wall current (e) can be expressed in the following way:

$$\dot{Q}_{flow,i\to e} = h_{c,air} A_{w,i} (T_i - T_w) \ , \tag{7}$$

where $h_{c,air}$ is the convection coefficient at the wall, T_w is the temperature of the wall and $A_{w,i}$ is the area of the vertical surface connecting layer (i) and the wall. Following the initial model formulation [18], this heat flux is rather formulated using the conservation of energy applied to the mass of air that leaves layer (i) to enter the wall current (e),

$$\dot{Q}_{flow,i\to e} = C_{p,air}\dot{m}_{flow,i\to e}(T_i - T_{flow,i\to e}), \quad (8)$$

using the mass flow from layer (i) to the flow element (e), $\dot{m}_{flow,i\to e}$, and the mean temperature of the wall current resulting from the air entering from layer (i), $T_{flow,i\to e}$. The zonal model approximates this last temperature by:

$$T_{flow,i\to e} \simeq 0.75T_i + 0.25T_w \ , \quad (9).$$

Substituting Eq. (9) into Eq. (8) and comparing the result to Eq. (7), the zonal model computes the mass flow from layer (i) to the flow element (e) using the following equation:

$$\dot{m}_{flow,i\to e} = 4h_{c,air}A_{w,i}/C_{p,air} \ , \quad (10)$$

The mass flow in the wall current (e) at the level of layer (i), $\dot{m}_{e,i}$, is the sum of $\dot{m}_{flow,i\to e}$ and the mass flow from layer (i+1) to layer (i) transported by the wall current, $\dot{m}_{de,i}$:

$$\dot{m}_{e,i} = \dot{m}_{de,i} + \dot{m}_{flow,i\to e} \ . \quad (11)$$

The corresponding wall current temperature at the level of layer (i) can be evaluated by the energy conservation:

$$T_{e,i} = (\dot{m}_{de,i}C_{p,air}T_{e,i+1} + \dot{m}_{flow,i\to e}C_{p,air}T_{flow,i\to e})/\left(\dot{m}_{e,i}C_{p,air}\right) . \quad (12)$$

The final step determines which fraction of $\dot{m}_{e,i}$ should continue in the lower layer (i-1) or be reintroduced to layer (i), $\dot{m}_{flow,e\to i}$, due to boundary layer detachment:

$$\dot{m}_{de,i-1} = p_i\,\dot{m}_{e,i} \ , \quad (13)$$

$$\dot{m}_{flow,e\to i} = (1-p_i)\,\dot{m}_{e,i} \ , \quad (14)$$

where p_i is computed for each layer (i) using the following rules:

$$p_i = \begin{cases} 0 & (T_{e,i} \geq T_i) \\ 1 & (T_{e,i} \leq T_{i-1}) \\ (T_i - T_{e,i})/(T_i - T_{i-1}) & (otherwise) \end{cases} \quad (15)$$

2.3 Thermal plume

The modelling of thermal plumes is based on the founding work of Morton et al. [29] for fully-developed turbulent free plumes in a quiescent environment. Using conservation equations and assuming a constant entrainment factor (α), ordinary differential equations enable to compute the axial evolution of the three main integral quantities: the plume volume flow (q_p), momentum (*m*) and buoyancy flux (*B*) [30]. In the following derivations, it is also assumed that the width of the velocity and temperature fields in a horizontal plane are the same.

The first two equations are common for every plume geometry,

$$dB/dz = -g\beta q_p (dT_\infty/dz) \ , \tag{16}$$

$$dm^2/dz = 2 q_p B \ , \tag{17}$$

where *z* is the axial direction, β is the coefficient of thermal expansion of air and T_∞ is air temperature of the environment. On the contrary, the last equation takes a different expression depending on the plume geometry. For an axisymmetric three-dimensional plume (3D), this equation is

$$dq_p/dz = \pi^{1/2} 2^{3/2} \alpha m^{1/2} \ , \tag{18}$$

while it takes the following form for a two-dimensional plane plume (2D),

$$dq_p^2/dz = 2^{5/2} \alpha m \ . \tag{19}$$

These plume equations are solved using the concept of virtual origin where a punctual source of buoyancy generates a plume similar to the real heat emitter. At this origin, $B(0)$ should be given as an input and equals to

$$B(0) = \frac{g\beta P_c}{\rho C_{p,air}} \tag{20}$$

where P_c is the instantaneous power emitted in form of convection by the heat emitter. At the origin, q_p and *m* are set very small but not null to avoid singularity of the plume equations. Selecting these initial conditions leads to a so-called pure plume. In conclusion, input parameters for the plume model are the plume geometry (i.e. 2D vs. 3D), the vertical location of the virtual origin above the floor, the entrainment factor (α) and P_c. The *symmetry* rule can be applied if the heat emitter is located along a wall [30]. With a wall, the entrainment of the plume is hindered on the side of the plume striking the wall surface. The plume is then modelled by two heat sources, the original one and an image reflecting the original one on the other side of the wall.

Electric radiators are in general narrow so that it is reasonable to assume that the plume is 2D and mostly pure. The case of wood stoves is more critical and deserves extended explanations. The dimensions of the stove are not small compared to the size of the room. Therefore, a significant distance is needed before the plume becomes fully developed above the stove. Furthermore, even after this establishment distance, the plume has still a deficit of momentum so that the plume is said to be lazy [31, 32] and not pure. It takes an additional distance for the lazy plume to converge to a pure plume. In order to confirm whether the plume model is valid for stoves, measurements of stove plumes have been performed in a large laboratory hall that can be assumed isothermal. Air velocity was measured using low-velocity anemometers and air temperature using thermocouples of type T. Results were reported in [33]. If the stove width is taken as the reference length, it takes approximately two to three times this distance above the stove before the plume is established. On the contrary, the plume is still not pure at 2 m above the floor so that one should consider that the plume remains lazy before reaching the ceiling of a room with standard dimensions. In conclusion, the assumptions of the plume model are not met in practice for space-heating using wood stoves. Nevertheless,

measurements showed that the model is still able to predict integral quantities correctly, such as the volume flow and the centreline temperature excess. These are the quantities that need to be introduced in the zonal model. In addition, these measurements confirm that the entrainment factor (α) is in the range of 0.1-0.13 (as reported in other case studies in the literature) and that the width of velocity and temperature fields are very similar. It was also proved that the virtual origin can be fairly approximated using an engineering rule of thumb, the *maximum* rule [34]. Consequently, the plume model can be reasonably applied for wood stoves in the zonal model and the only input parameter left is P_c. If the virtual origin is located below the stove's lowest horizontal surface ($z_{\min}$), the effect of the plume is only accounted for in air layers located above $z_{\min}$.

In the zonal model, the plume mass and energy are entirely injected within the top air layer of the room. In reality, the plume impinges on the ceiling so that this wall receives energy from the plume directly. This effect is not accounted for using the present zonal model where the energy of the plume is fully injected into the top air layer and can only influence the ceiling temperature indirectly.

2.4 Implementation

It has been decided to implement the zonal model in MATLAB in order to facilitate its development and, if necessary, to be able to quickly test alternative formulations. In IDA ICE, the zonal model is implemented in an equation-based object-oriented environment [35] which makes the question of the resolution of the model equations less relevant. The implementation in MATLAB is specific to the test cell geometry and, to date, cannot support other geometries. Each wall of the test cell is assumed isothermal with a uniform surface temperature, T_w. The geometry of heat emitters is modelled by a box. The six surfaces of this box can have different temperatures. Nevertheless, a same surface temperature (T_s) is imposed in the present work. Assuming that the air and wall temperature fields are known at time step (n) (i.e. T_i^n, T_s^n and T_w^n), model equations are integrated in time in the following way:

1. The convective power of the heat emitter (P_c^n) is evaluated using correlations. This is a necessary input to evaluate the plume in step 2. These correlations will be introduced in Section 3, describing the experimental setup.
2. Flow elements are computed for the wall boundary layers and the plume of the heat emitter. The output of the evaluation of flow elements enables to evaluate Eqs. (2) and (6).
3. The conservation of mass, Eq. 1, is used to compute the net mass flow between layers, $\dot{m}_{lay,i}$.
4. The conservation of energy, Eq. 3, is integrated in time using an explicit Euler method. It gives the value of the air temperature at the next time step, T_i^{n+1} .
5. The longwave radiation between internal walls of the test cell (P_r^n), including the surfaces of the heat emitter, is evaluated using the radiosity method. The view factors between internal walls have been computed beforehand using a numerical method [36].
6. For each internal wall of the test cell, the convective and radiative heat fluxes to the wall (taken from step 2 and 5, respectively) are summed up to form the total heat flux to the wall, P_{tot}^n.
7. The measured air temperature around the test cell at time step (n) and P_{tot}^n serve as boundary conditions for the heat transfer inside the wall. The walls of the test cell are composed of several

layers. The thermal properties of the wall materials are assumed homogeneous and constant for each layer. The one-dimensional heat diffusion equation is discretized in space using second-order finite volumes and integrated in time using an implicit Euler method. This enables to evaluate the wall temperatures at the next time step, T_w^{n+1}.

A convergence analysis has been performed to determine an acceptable number of air layers (N), discretization points for each wall layer (N_w) and time step (Δt). This lead to N = 32, N_w = 10 and Δt = 5 seconds.

The default model parameters proposed in the original paper of Togari have been used [18]. In particular, the convective heat transfer coefficient of internal walls of the room, $h_{c,air}$ in Eq. (10), has been assumed constant. Following Togari's recommendation for natural convection, $h_{c,air}$ is taken equal to 3.5 W/m².K for vertical walls, 2.3 W/m².K for heating from a ceiling and cooling from a floor, and 4.6 W/m².K for cooling from a ceiling and heating from a floor. The effective thermal conductivity of air in Eq. (4) is taken equal to the physical one assuming that the effect of the background turbulence is negligible on temperature mixing.

3 Experimental setup

3.1 ZEB Test Cell

The experiments were conducted in a test cell located in Trondheim, which is described in Figure 3. The test cell has one external wall with a window while the other walls are surrounded by a guard zone inside a building. The air in the guard zone was circulated with fans to assure uniform temperature distribution. The test cell was not ventilated during experiments.

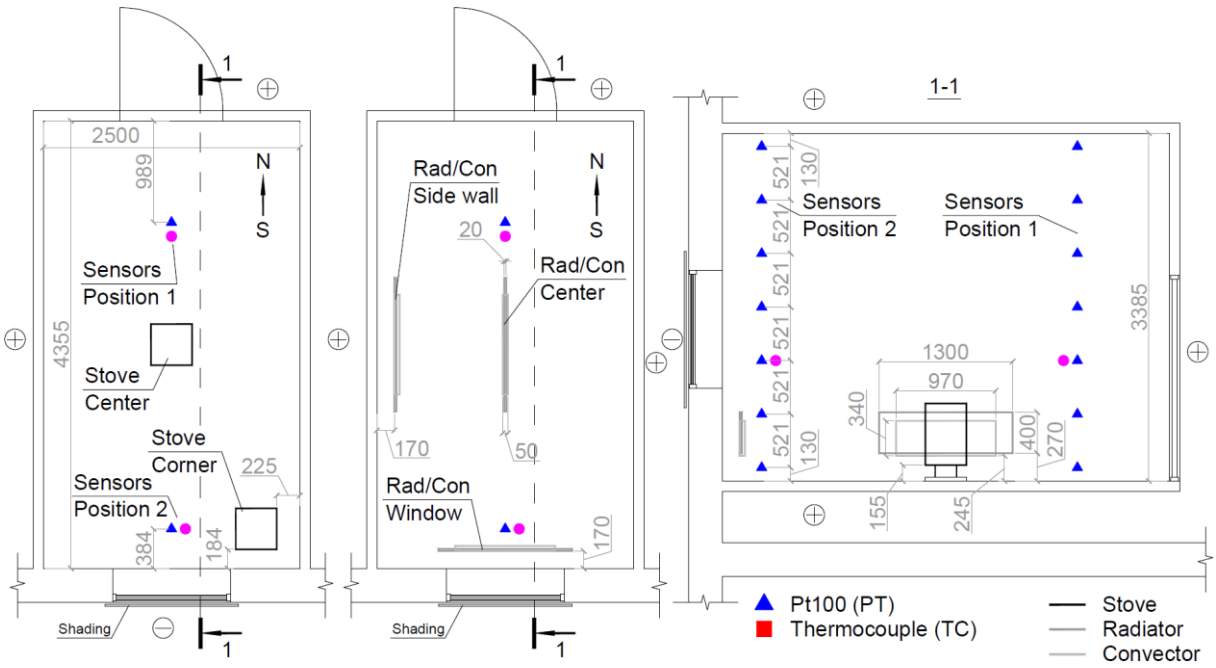

Figure 3. The test cell geometry and dimensions as well as the location of the heat emitters and the Pt100 temperature sensors.

Two vertical poles were equipped with seven Pt100 temperature sensors and one Pt100 sensor inside a black globe of 70 mm external diameter per pole. These two poles were placed near the door and near the window (see Figure 3). The window was covered with a fixed opaque shading to reduce the impact of solar radiation. The space between the shade and window was ventilated with a vertical air gap of 20 mm. Detailed information about the test cell envelope is given in Tables 1 and 2. A triple pane window has been installed in the external wall. The total thermal transmittance of the glazing and frame are 0.66 and 2.7 W/(m^2·K), respectively. With a frame ratio of 14%, it results in a total value of 0.95 W/(m^2·K). The solar heat gain coefficient of the glazing is 0.34 and 0.03 without and with shading, respectively. The specific heat loss of the external wall including the window was 2.54 W/K, out of which 0.36 W/K were linear thermal bridges. The specific heat loss of the internal structures was 13.46 W/K. The emissivity of all internal surfaces was measured to 0.9 using an infrared camera. T-type thermocouples were installed on all internal surfaces of the test cell (1 to 5 sensors per surface). Additional T-type thermocouples were installed on the outside surface of the test cell in the guard zone to monitor the ambient condition around the test cell. The outdoor temperature, relative humidity, wind speed and direction as well as the solar radiation were measured by a weather station located on site. Global solar radiation was measured on horizontal and vertical south-facing planes. The parameters of the measurement equipment are given in Table 3. The heterogeneous mix of temperature sensors results from the different ranges of temperatures to be measured and from the use of different experimental setups (i.e. the test cell and the electric stove).

Table 1. The description of internal structures of the test cell.

Material	Thickness, mm			Thermal conductivity, W/(m·K)	Density, kg/m^3	Specific heat, J/(kg·K)
	Wall/Ceiling	Floor	Door			
Layer order: Test cell to outdoor air						
Wood	-	15	-	0.15	1250	1200
Steel	0.6	0.6	0.6	62	7800	500
PUR foam	98.8	98.8	78.8	0.03[a]	35	1600
Steel	0.6	0.6	0.6	62	7800	500

[a] – the thermal conductivity of polyurethane (PUR) foam was increased from 0.024 to 0.03 W/(m·K) to take into account the thermal bridges in the internal structures.

Table 2. The description of the external wall: R of air cavity means the thermal resistance of the layer.

Material	Thickness, mm	Thermal conductivity, W/(m·K)	Density, kg/m^3	Specific heat, J/(kg·K)
Layer order: Test cell to outdoor air				
Wood	5	0.15	1250	1200
Glasswool	300	0.035	32	670
Air cavity	0.02	R=0.18 (m·K)/W	1.2	1007
Cladding	5	0.5	1250	1200

Table 3. The description of measurement equipment (TC stands for thermocouple).

Type	Position	Physical variable	Accuracy	Sampling time
Pt100	Test cell	Air temp.	±0.1 K	1 min
TC type K	Stove surface	Surface temp.	±2.2 K	5 sec
TC type T	Test cell surface	Air/surface temp.	±0.4 K	5 sec/1 min[a]
Pt100	Weather station	Air temp.	±0.15 K	5 sec/1 min[a]
Pyranometer	Weather station	Global irradiance	2nd Class	5 sec/1 min[a]

[a] – during experiments, 5 seconds, and 1 minute between experiments.

The analysis of measurement results revealed limitations in this experimental setup. Firstly, quick temperature variations were imposed on the test cell so that the black globes were not able to follow these rapid changes: the response time for the black globes was estimated to be about 15 minutes. Therefore, it was decided to reconstruct the mean radiant temperature at the level of the black globes (T_{mrt}) using the measured wall surface temperatures (including the heat emitter surfaces) and view factors. Secondly, thermocouples on wall surfaces were covered by a reflective tape. This had no influence on most of the walls as their first internal layer has a good thermal conductivity (i.e. made of steel). Nevertheless, this was critical for the floor because of its first layer of wood, which has lower thermal conductivity. Significant errors were thus expected regarding the measurement of the floor temperature.

During experiments, the outdoor temperature ranged between 0.9 and 10.5 °C. The guard zone temperature was stable, ranging between 19.8 and 22.3 °C. Solar radiation did not have significant impact on experiments due to the shaded window and well-insulated external wall.

3.2 Electric radiators

Two types of on-off electric radiators available on the market have been considered. Firstly, a convector of 1 kW and with a dimension of 0.97 m x 0.05 m x 0.34 m was tested. In convectors, the electric resistance is placed in a channel constructed using metallic plates in order to enhance the thermal draft. Most of the heat is thus expected to be emitted by convection. Nevertheless, preliminary laboratory measurements revealed that the external surface temperature of this commercial convector is not low (i.e. about 55°C above the room air temperature) so that a significant part of the heat is still emitted by longwave radiation. Based on these laboratory measurements, the convector surface temperature (T_s) is evaluated in the following way:

$$T_s = 55(1-\exp(-t/200)) + \overline{T}_{air}, \tag{21}$$

where *t* is the time (given in seconds) after the convector started and $\overline{T}_{air}$ is the volume-averaged air temperature of the room. Using T_s, it is possible to estimate the amount of heat emitted by longwave radiation assuming that the convector is small compared to the room size [37]:

$$P_r \approx \sigma \varepsilon A_s (T_s^4 - \overline{T}_{air}^4), \tag{22}$$

where σ is the Stefan-Boltzmann constant, ε is the surface emissivity (identified at 0.9 using an infrared camera) and A_s is the total area of the convector external surface. In this last equation, temperature is expressed in Kelvin. The power emitted by convection is then estimated as follows:

$$P_c = 1000(1-\exp(-t/200)) - P_r \ . \tag{23}$$

Secondly, an airtight electric radiator of 800 W with dimensions of 1.3 m x 0.02 m x 0.4 m was considered. The electric resistance is in close contact with the entire external surface of the radiator. Unlike convectors, there is no airflow through the radiator. Based on preliminary laboratory measurements, the total emitted power is approximated by

$$P_{tot} = 800(1-\exp(-t/240)) \ . \tag{24}$$

The surface temperature (T_s) expressed in Kelvin is estimated by solving the following non-linear equation:

$$P_{tot} = P_c + P_r = 1.22 A_s (T_s - \overline{T}_{air})^{4/3} + \sigma \varepsilon A_s (T_s^4 - \overline{T}_{air}^4). \quad (25)$$

The first term of Eq. (25) corresponds to the heat emitted by convection (P_c) and is based on the Churchill and Chu correlation for a laminar and turbulent boundary layer over a vertical plate [38]. The emissivity was identified at 0.9 using an infrared camera.

3.3 Electric stove

The electric stove is a box of 0.4 m x 0.4 m x 0.6 m. Its maximum electric power is 4.1 kW. The stove surface is equipped with electric heating plates mounted on 50 mm of heatproof thermal insulation so that most of the heat that is delivered to the plates is emitted towards the room (and not stored inside the stove). All stove surfaces were painted to get a uniform emissivity of 0.9, which was again verified using an infrared camera. This stove is a smaller version of an existing electric stove used in previous investigations [26].

The temperature of the stove surfaces was controlled. In the middle of each surface, the temperature was measured using a thermocouple of type K. This temperature is given as an input to a PI controller that regulates the input signal to a thyristor. Based on this input signal, the thyristor modulates the power of electric resistances. In this way, the temperature is continuously controlled to a predefined set-point temperature profile. All six stove surfaces can be controlled independently, which is important to reproduce realistic temperature distributions over the external surface of a wood stove. Nevertheless, a same set-point temperature (T_s) is imposed in the present study for the six surfaces of the electric stove.

As introduced in Subsection 2.4 (step 1), it is necessary to be able to evaluate the power emitted by convection (P_c) as a function of the stove surface temperature (T_s). A correlation has been established based on preliminary experiments in a large hall. A constant set-point temperature was imposed to the stove surfaces until it reaches a steady-state regime. In this regime, the electric power equals the total power emitted by the stove (by convection and longwave radiation). The laboratory hall is large compared to the stove dimensions and can be considered isothermal during these experiments. Therefore, the fraction of power emitted by thermal radiation (P_r) can be easily estimated using Eq. (22). For a given stove T_s, P_c is then obtained by subtracting the estimated thermal radiation from the measured electric consumption. A similar procedure was used in the previous study using a larger electric stove [26]. In both cases, the convective power (P_c) can be fairly approximated by the Churchill and Chu correlation for a laminar and turbulent boundary layer over a vertical plate [38]:

$$P_c = 1.22 A_s (T_s - \overline{T}_{air})^{4/3}, \quad (26)$$

where A_s is the total area of the stove external surface.

3.4 Test cases

The convector and radiator were operated at full power (i.e. without thermostat) during cycles of 72 and 90 minutes, respectively, to achieve an equal amount of energy emitted to the room. Cases with a central position in the room as well as parallel to a wall in the test cell were tested. In this last case, the convector and radiator were placed 17 cm away from the wall. This distance is relatively large compared to real applications but it has been set for security reasons (i.e. to prevent high temperatures at the wall). In order to limit the duration of the experimental campaign, a maximum of two experiments were performed per day. Between two experiments, the position of the heat emitter was changed in the room. Unfortunately, it turned out that the opening of the test cell door when shifting position impacted the thermal environment of the room significantly so that the initial conditions before the second daily test were unclear. After a detailed analysis of experimental results, only the first daily experiment appeared to be enough consistent. This corresponds to the convector in a central position and the radiator along an internal wall.

Regarding the electric stove in a central position, 8 different set-point profiles for the surface temperature were investigated in order to create a large range of thermal stratifications and cycle lengths. These profiles are given in Figure 4. The surface temperatures are representative for real wood stoves but the length of the cycles were relatively shorter. This is due to the small dimensions of the test cell: longer cycles with such high surface temperatures would have led to unrealistic indoor temperatures (above 30°C). Four temperature profiles were tested for the stove located in a corner, 20 cm away from the walls.

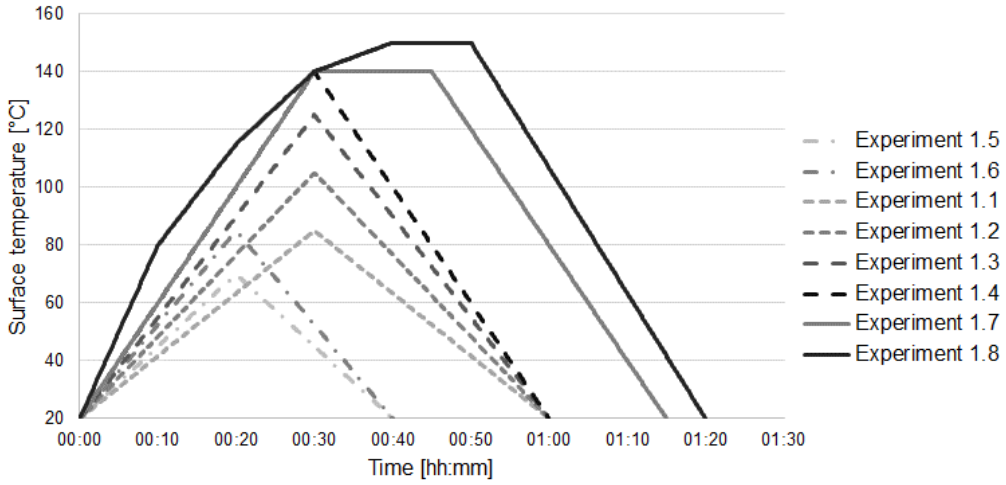

Figure 4. The set-point profiles of the stove surface temperature (T_s) used in experiments with the electric stove in a central position in the room.

4 Results

4.1 Calibration of the effective specific heat

The test cell is equipped with a large metallic box for electric connections. In addition, sensors were placed on two vertical steel bars fixed on a metallic base. The data loggers of the wireless Pt-100 sensors were also attached on a vertical metallic plate. After preliminary tests of the zonal model, it turned out that the corresponding thermal mass could not be neglected. As these metallic plates are thin, their thermal mass has been associated to the effective specific heat of the room air, $C_{p,eff}$. To identify this last value, test case 1.8 with the electric stove has been simulated using the standard room

model (i.e. isothermal air in the room). The calibrated thermal capacitance has been evaluated at 120 kJ/K for the entire room volume. This corresponds to circa 60 kg of metal, which is in line with the experimental setup. The resulting thermal response of the isothermal room is shown in Figure 5 for the air temperature and the mean radiant temperature (T_{mrt}) calculated at the position of the two black globes. In the zonal model, the effective thermal mass of 120 kJ/K has been distributed evenly between all the layers.

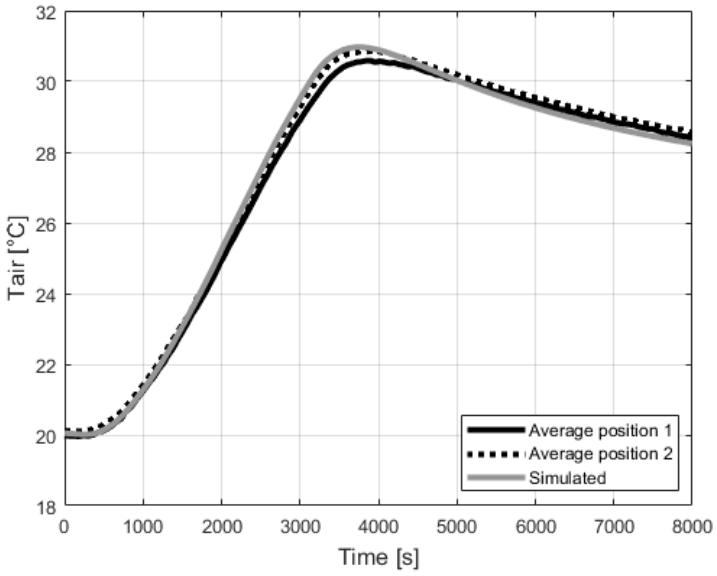

(a)

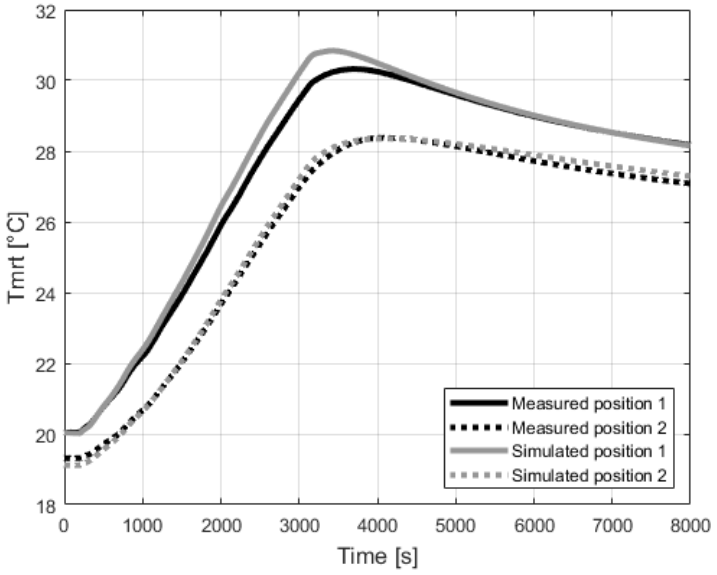

(b)

Figure 5. Calibration of the effective specific heat ($C_{p,eff}$) of air using the standard room model.

4.2 Stove in central position

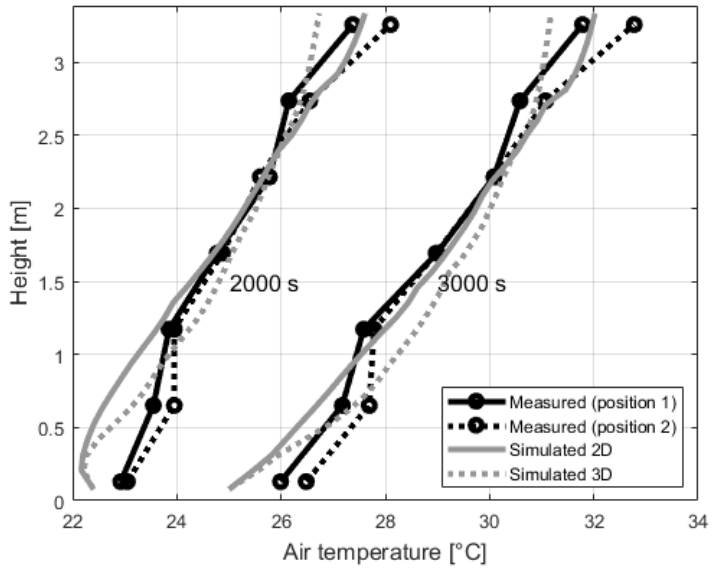

(a)

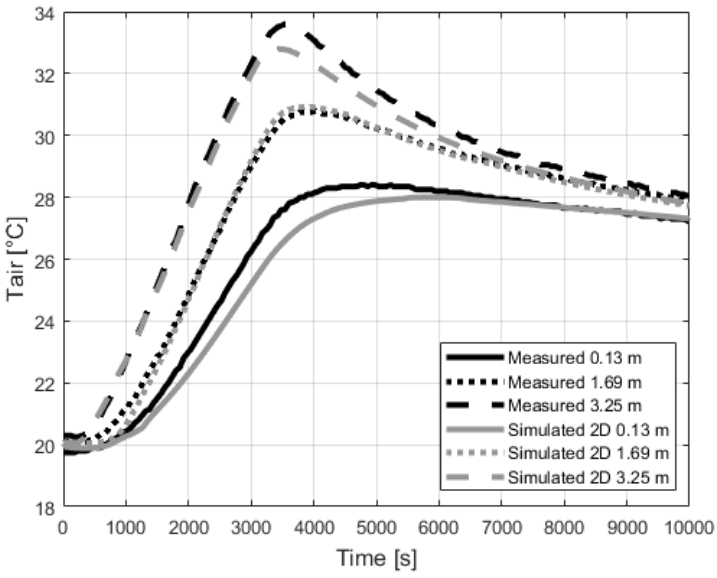

(b)

Figure 6. Measured and simulated vertical air temperature distribution for test case 1.8: simulations were done using a three-dimensional axisymmetric (3D) and two-dimensional plane (2D) plume.

The case of the stove in a central position is first analysed. A single test case is selected to illustrate results. Test case 1.8 has the longest operation cycle and the highest maximum surface temperature of the stove (i.e. 150°C). Results of this last case are representative for the performance of the 7 other tests. Again, the dimensions of the stove are not small compared to the room size, especially the 2.5 m width. It is thus questionable to assume that the plume expands freely in its environment in such a small room. This would correspond to a three-dimensional axisymmetric plume (3D). Computational Fluid Dynamics (CFD) have been performed in order to verify the plume geometry. The computational setup and results are given in the Appendix. It turns out that the plume is constrained and that a two-

dimensional plane plume (2D) better predicts the evolution of the mass flow and centreline excess temperature of the plume. The air stratification using the 2D and 3D plumes is shown in Figure 6(a), 2000 and 3000 seconds after the heating started. Results are similar for both plumes, but the 2D plume better predicts the stratification. For this test case, the remaining results will be presented for the 2D plume. The stratification is particularly well predicted above the stove top surface (i.e. 0.75 m above the floor) but poorer below that level. Figure 6(b) confirms that the dynamics of the stratification is correctly reproduced.

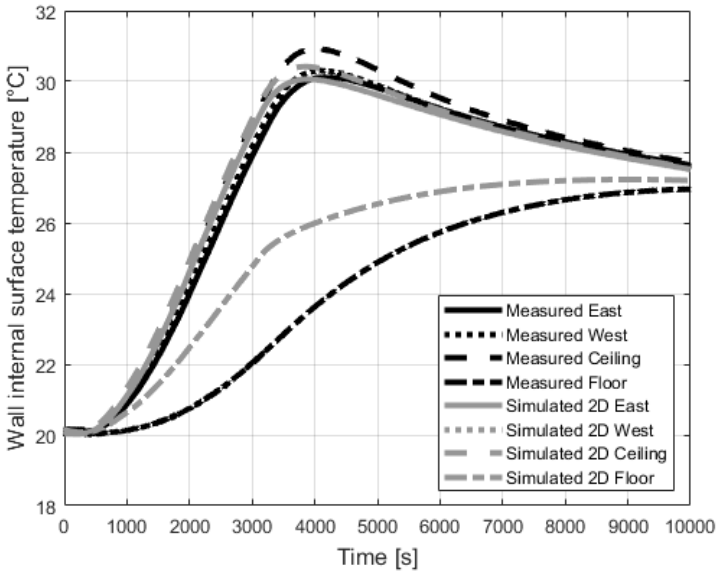

(a)

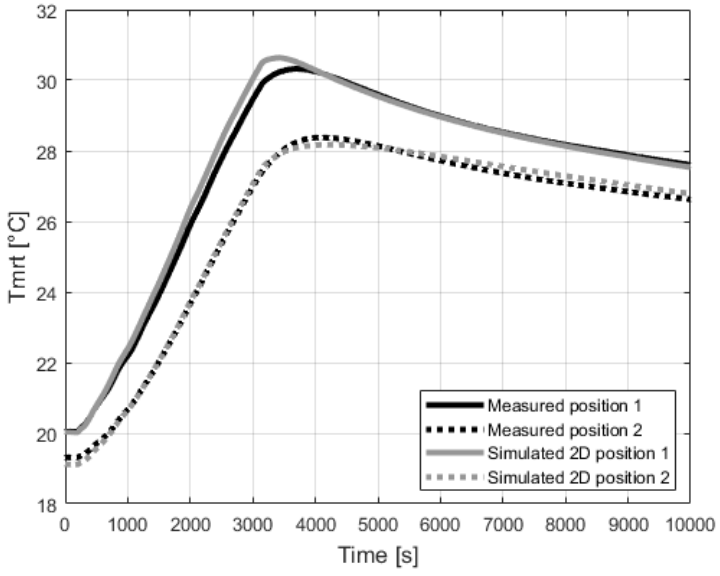

(b)

Figure 7. Measured and simulated internal surface temperatures for test case 1.8 and the resulting mean radiant temperature.

The time evolution of the internal surface temperatures of the test cell walls is shown in Figure 7(a). As already discussed, the floor temperature is not accurately measured so that it is difficult to conclude

about the accuracy of its prediction. For other surfaces, walls temperatures are well reproduced by the zonal model. The ceiling temperature is slightly under-predicted but it can be explained by the plume modelling at the level of the ceiling. In reality, the plume impinges on the ceiling while this effect is not accounted for in the zonal model. Figure 7(b) shows that the mean radiant temperature is remarkably well predicted by the zonal model. As the stratification and the mean radiant temperature are well captured by the model, the operative temperature is also well reproduced.

4.3 Convector in central position

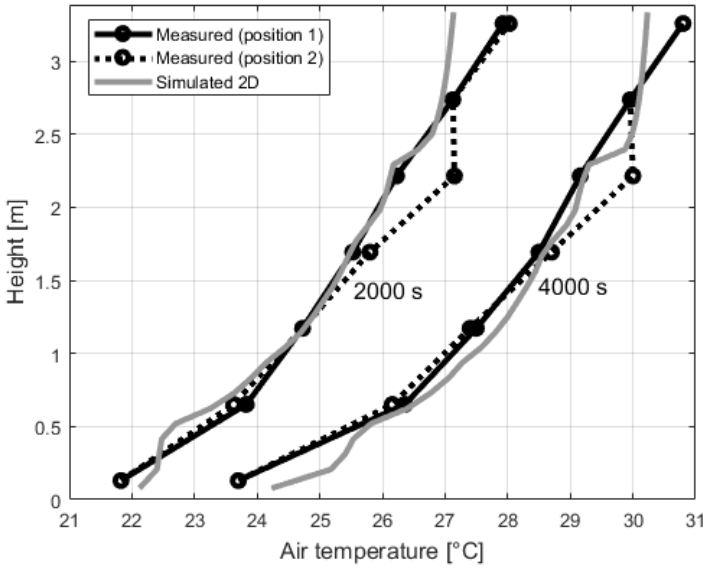

(a)

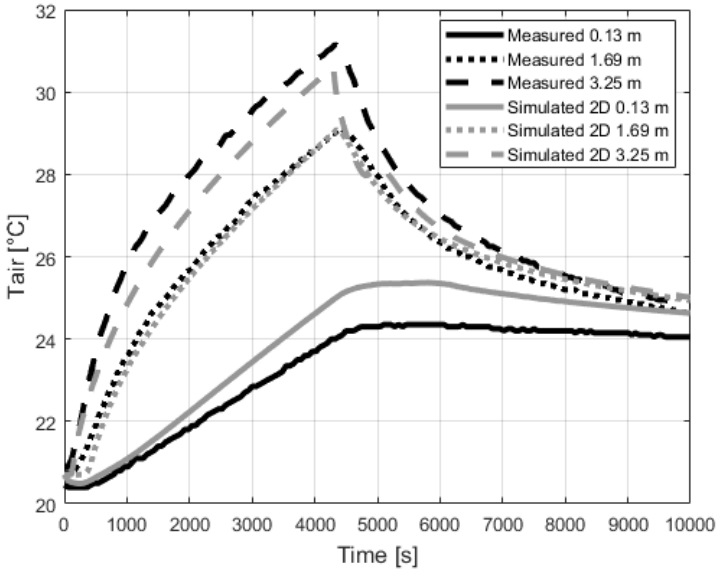

(b)

Figure 8. Measured and simulated vertical air temperature distribution for the convector in a central position.

The performance of the convector in a central position is shown in Figures 8 and 9. The stratification is well reproduced by the zonal model, especially in the middle of the room and less near the ceiling

and the floor. The model is able to follow the dynamics of the stratification even though temperature changes are relatively quick (for example, the temperature of the top air layers increases with ~10°C in one-hour time). For the sake of article conciseness, wall temperatures will not be shown, only the resulting mean radiant and operative temperatures will be analysed. Figure 9 proves that the zonal model is able to reproduce the dynamics of these two temperatures.

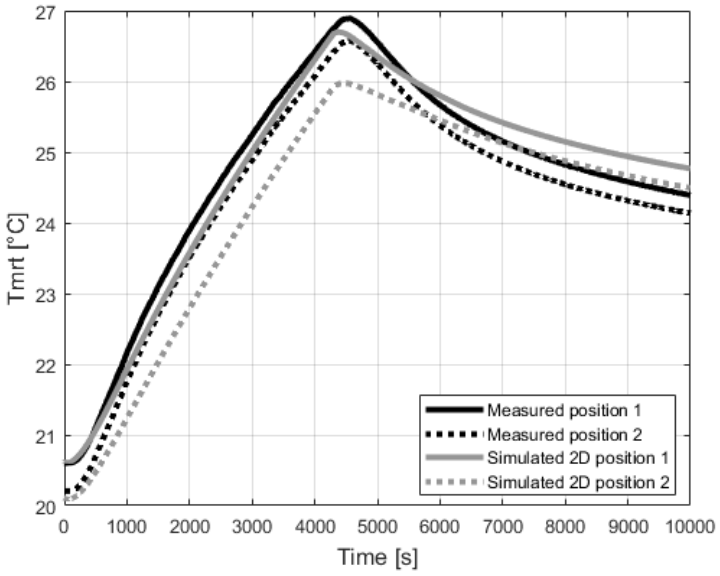

(a)

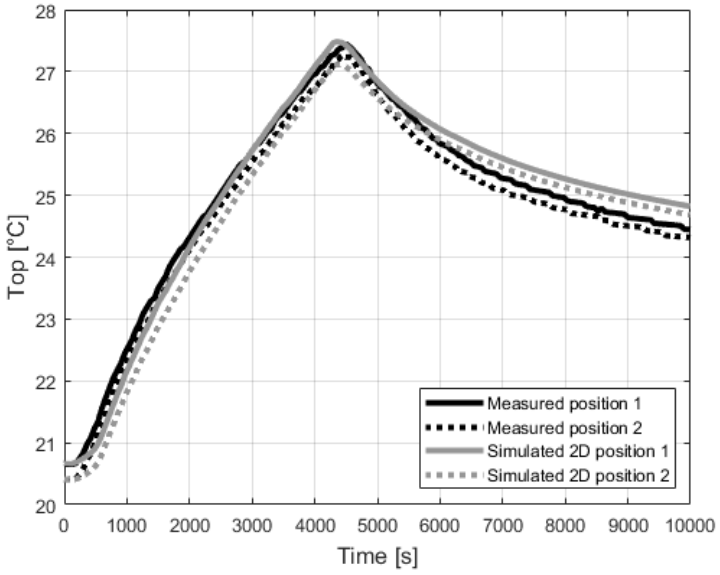

(b)

Figure 9. Mean radiant and operative temperatures for the convector in a central position.

4.4 Radiator along wall

The performance of the electric radiator along the west wall is shown in Figures 10 and 11. As for the previous cases, the stratification is remarkably well reproduced. On the contrary, Figure 11(a) shows that the temperature of the west wall is significantly overestimated by the zonal model. It leads to a mean radiant temperature which is overpredicted for the black globe that is the most exposed to the

west wall, the globe near the door. This behaviour can be explained by the modelling assumptions. The entire west wall is assumed isothermal and the longwave radiation of the radiator is distributed evenly over this wall. In reality, the thermal radiation would be more intense in the direct vicinity of radiator leading to a non-uniform wall temperature.

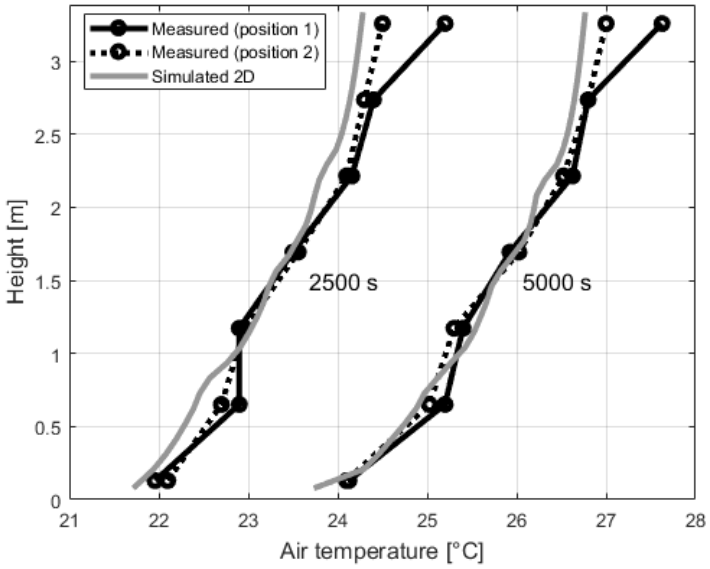

(a)

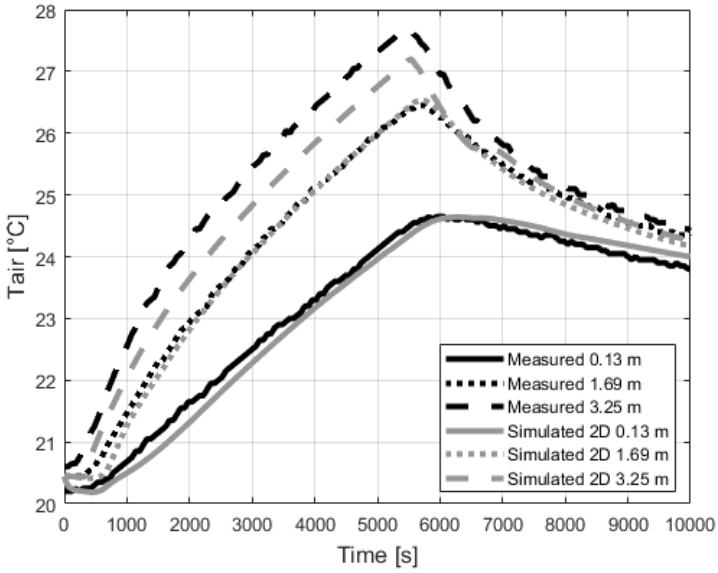

(b)

Figure 10. Measured and simulated vertical air temperature distribution for the radiator located along the west wall.

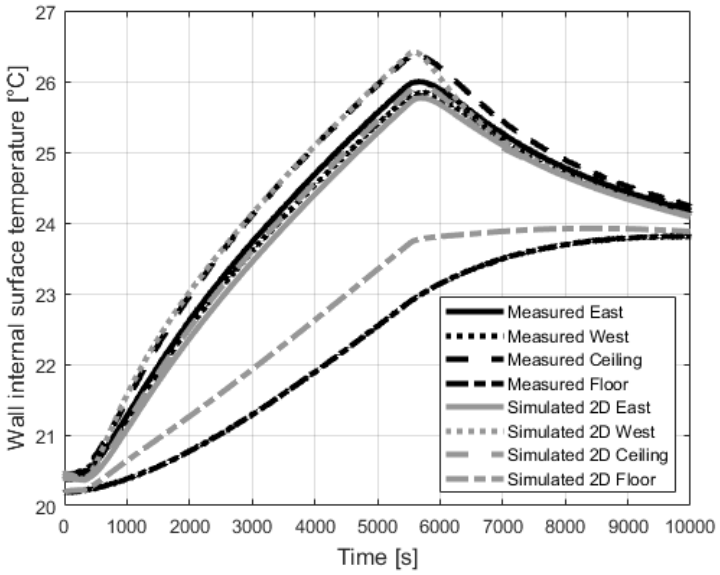

(a)

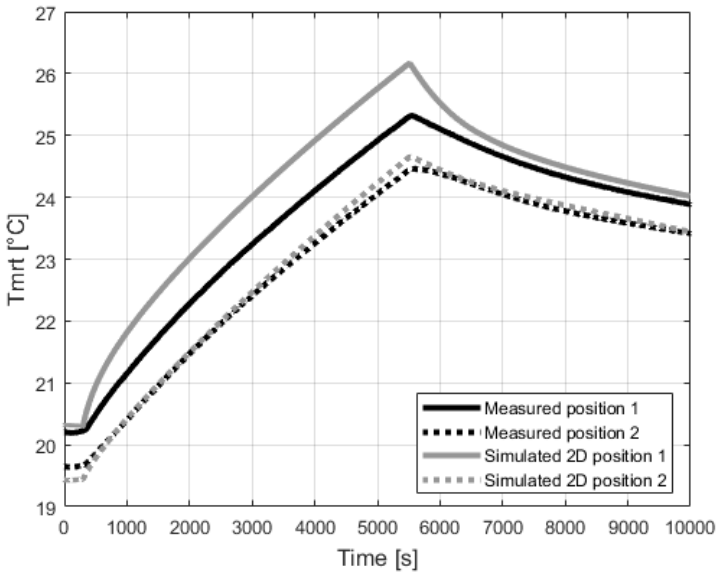

(b)

Figure 11. Measured and simulated internal surface temperatures for the radiator along the west wall and the resulting mean radiant temperature.

The case of the stove located in a corner is not shown because it leads to similar conclusions as for the radiator along a wall: the stratification is well predicted but the internal surface temperature is not well enough reproduced in the vicinity of the heat emitter.

5 Discussion

Several comments can be given regarding the experimental setup and the performance of the zonal model:

- In all experiments, the air temperatures measured for a same height but at the two different horizontal locations were very similar, proving that the air temperature distribution in the room is essentially one-dimensional. This is in line with the zonal model assumption.
- The effective heat capacitance ($C_{p,eff}$) of the room has been estimated to be 120 kJ/K, corresponding to 75 kJ/K if the contribution of the air is removed. An important question is to determine whether this value of 75 kJ/K, or 6.88 kJ/K.m² of floor area, is representative for the internal thermal mass of real buildings, such as furniture. Values reported in the literature are significantly higher (> 10 kJ/K.m²) [39] but based on longer time responses than considered in our investigations. As they typically resort to daily responses, it is therefore not astonishing that the literature reports higher values. To the author's knowledge, default (or standardized) values of internal thermal mass for short-term temperature changes are not available.
- Taking $C_{p,eff}$ equal to $C_{p,air}$, the stratification predicted by the zonal model for the stove case is significantly different using the three-dimensional axisymmetric and two-dimensional axial plumes. This suggests that, for low internal thermal capacitances, the shape of the stove plume should be known.
- It is very unlikely that users will install such a powerful heat source, like the electric stove, in a small room. In real applications, the stove is most probably placed along a wall in a large room. Further investigations of the stove plume in such configurations are required, using measurements or CFD. Given the typical safety distance between a stove and its surrounding walls, one can expect the plume to be free (meaning not attached to the wall) so that a three-dimensional axisymmetric plume should be the best candidate. Nevertheless, the proximity of the walls may alter the entrainment factor of the plume.
- It can be argued that a CFD simulation is not sufficient proof that the plume is 2D in the test cell. Indeed, a CFD simulation can also be prone to numerical and turbulence modelling errors. Nevertheless, it has been shown in Figure 6(a) that the 2D plume better predicts the thermal stratification than the 3D plume in the test cell. Although this argumentation is not a demonstration that the plume is 2D (plume measurements in the test cell would be necessary), this is nonetheless an additional valuable evidence.
- The zonal model proved to be able to reproduce the dynamics of the stratification even for the short but intense space heating cycles investigated in this article. Such short periods with large indoor temperature increases are frequently proposed in the context of thermal mass activation and building energy flexibility, see e.g. [40]. It means that the zonal model is a good candidate to investigate the detailed indoor thermal environment in the context of demand side management (DSM) and thermal mass activation.
- The default parameters of the Togari model for natural convection have been used. No adjustment of the model parameters has been made to match experimental results. The effective heat capacitance of the room has been calibrated but assuming the standard room model, not the zonal model. These investigations suggest that the default parameters in the Togari model could be applied for a large range of applications. This is valuable information in the context of a commercial use of the zonal model.
- In future work, the experimental setup could be improved. Larger rooms should be considered and the wall surface temperature in the vicinity of the heat emitter should be investigated. In addition, alternative methods to black globes should be used in order to measure the mean radiant temperature during rapid temperature variations. In the present work, the mean radiant temperature has been reconstructed using wall temperatures and view factors. Furthermore, measurements of the floor surface temperature were inaccurate due to the installation of a reflective tape. This typically leads to an error of one degree. Therefore, the influence of this error

on the measured mean radiant temperature is limited. Finally, measurements of the stove plume could be added.

- In the presence of a heat emitter near a wall, the article shows that the entire wall cannot be considered isothermal, for instance to properly predict the mean radiant temperature. Further research is needed to propose automated methods to split the wall into many isothermal parts. Splitting the wall into many parts is easily supported by the architecture of the room model in IDA ICE. On the contrary, it would necessitate a significant rewriting of the present MATLAB implementation.

6 Conclusions

In building performance simulation (BPS), zonal models are intermediate models between standard models assuming perfectly-mixed room air and Computational Fluid Dynamics (CFD): they aim to predict the temperature and velocity fields as well as the pollutant distribution inside a room using a computational time significantly lower than CFD. The present article aims at validating a transient zonal model that is currently implemented in the commercial BPS tool, IDA ICE. In theory, this one-dimensional model can address a large variety of airflows and requires almost no *a priori* knowledge of the flow to be computed. These are important criteria for the implementation in a commercial BPS tool. The zonal model has already been validated in the past for different flow benchmarks with encouraging results, but the need for further validations was clearly stressed.

In this article, the zonal model is validated against measurements in a room heated by either electric radiators or an electric stove designed to mimic surface temperatures of real stoves. Using an electric stove enables to estimate the heat emitted to the room accurately. This would be challenging using a real wood stove while it is a necessary information to validate the zonal model. Unlike electric radiators, the case of stoves has never been addressed in the literature and is challenging due to the strong thermal coupling between the room air and walls. Heat emitters have been placed either in the middle of the room or along walls.

During experiments, the air temperature was increased rapidly. It was therefore important to correctly identify the effective thermal capacitance associated to the room air. In the laboratory, this capacitance is mostly associated to the measurement equipment installed in the room but, in real applications, this capacitance would correspond to furniture. Investigations also showed that the geometry of the stove plume has a small but non-negligible effect on results. The laboratory was not large compared to the stove size so that the plume could not be assumed free: the stove plume behaved more like a two-dimensional plane plume than a three-dimensional axisymmetric plume. In real applications, the room would be significantly larger than the one used for experiments. Given the typical safety distance between a stove and its surrounding walls, one can expect the plume not to be attached to its neighbouring wall so that a three-dimensional axisymmetric plume should be the best candidate. The proximity of the wall may nonetheless alter the entrainment factor of the plume. Consequently, further investigations are required regarding the plume geometry in real applications.

The zonal model has been applied using the default model parameters. No attempt has been made to tune these parameters to improve the model performance. The zonal model remarkably predicted the time evolution of the air temperature stratification in the room for all test cases. For a heat emitter in a central position, the wall surface temperatures were also predicted correctly. Nevertheless, for a heat emitter along walls, these walls cannot be considered isothermal anymore, an assumption found in most BPS tools. The paper suggests that an automatized method to divide walls in the vicinity of heat emitters would be necessary and convenient for a reliable prediction of the wall surface temperatures and the mean radiant temperature. Finally, these results further confirm that the zonal

model is a good candidate for an implementation in a commercial BPS tool and that validation should be continued using other categories of airflows as well as field measurements.

7 Acknowledgement

The authors acknowledge the financial support by the Research Council of Norway and a number of industrial partners through the project WoodCFD ("*Clean and efficient wood stoves through improved batch combustion models and CFD modelling approaches*").

8 Appendix

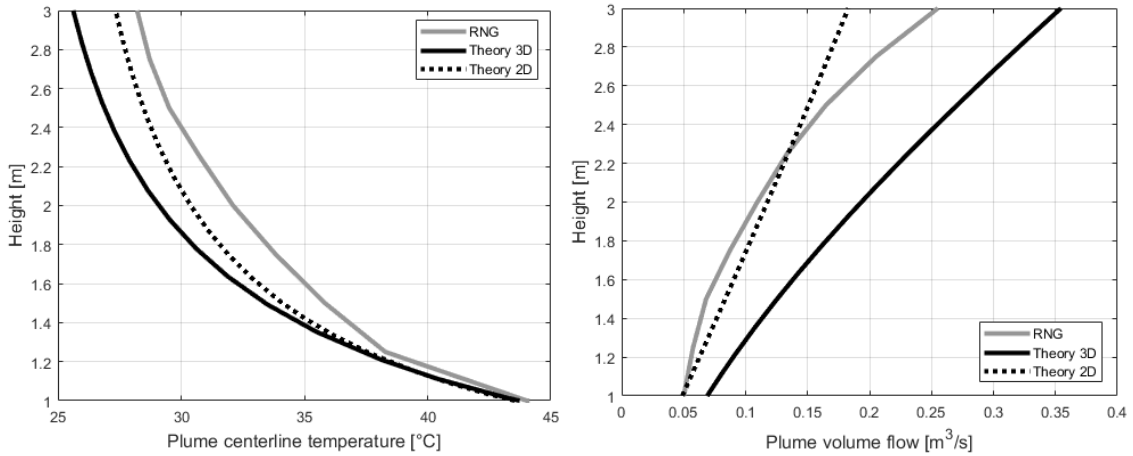

Figure 12. Unsteady RANS using the RNG k-ε model compared to the plume model (theory): three-dimensional axisymmetric (3D) and two-dimensional plane (2D) plume.

The geometry of the plume is a required input in the plume model. The width of the test cell is 2.5 m so that the distance between the stove and the nearest walls is only 1.05 m, about 2.5 times the width of the stove. The plume is thus probably not free to expand in its environment. In order to determine the plume geometry, a CFD simulation has been performed using Fluent. The temperature for all the internal surfaces of the test cell has been fixed to 20°C while a constant stove surface temperature of 150°C was imposed. A Reynolds-Averaged Navier Stokes (RANS) turbulence model has been considered, here using the RNG k-ε model. This RANS model is often said to be the most universal for airflows inside buildings, with good performance for many categories of airflows [5, 6]. As many flow phenomena take place simultaneously in our experiments (i.e. thermal plume, impingement of plume on the ceiling leading to an attached jet and boundary layers), the RNG k-ε model should be the most robust. Given the geometry of the stove, its plume is strongly unsteady. Steady RANS was not able to converge so that unsteady RANS (URANS) was considered, as recommended by Fluent guidelines. The solution is assumed converged when the residual for the equation of mass conservation is sufficiently low and when the time series of the flow diagnostics are statistically converged. Boundary layer meshes have been used along walls. The first point is located at a y+ of 1 while the increasing factor of the mesh size normal to the wall is 1.1. A tetrahedral mesh has been used with 11.5 million elements.

Figure 12 shows the evolution of the volume flow (q_p) and centreline air temperature along the plume axis. CFD results are compared to the plume theory assuming a three-dimensional (3D) axisymmetric and two-dimensional (2D) plane plume. In each case, an entrainment factor (α) of 0.1 has been used. The virtual origin has been chosen to have a same centreline temperature just above the stove, in the CFD and the plume model. The visualizations of the computed temperature field correspond to a 2D plume and Figure 12 confirms that the 2D plume model gives a better match with CFD.

9 References

1. Chen, Q., *Ventilation performance prediction for buildings: a method overview and recent applications.* Building and Environment, 2009. **44**: p. 848-858.
2. Srebric, J., *Ventilation performance prediction*, in *Building Performance Simulation for Design and Operation*, J.L.M. Hensen, Lamberts, R., Editor. 2011, Spon Press: Oxon. p. 143-179.
3. Wang, L. and Q. Chen, *Evaluation of some assumptions used in multizone airflow network models.* Building and Environment, 2008. **43**(10): p. 1671-1677.
4. Nielsen, P.V., *Fifty years of CFD for room air distribution.* Building and Environment, 2015. **91**: p. 78-90.
5. Zhai, Z.J., et al., *Evaluation of Various Turbulence Models in Predicting Airflow and Turbulence in Enclosed Environment by CFD: Part 1, Summary of Prevalent Turbulence Models.* HVAC&R Research, 2007. **13**(6): p. 853-870.
6. Zhang, Z., et al., *Evaluation of Various Turbulence Models in Predicting Airflow and Turbulence in Enclosed Environment by CFD: Part 2, Comparison with Experimental Data from Literature.* HVAC&R Research, 2007. **13**(6): p. 871-886.
7. Megri, A.C. and F. Haghighat, *Zonal Modeling for Simulating Indoor Environment of Buildings: Review, Recent Developments, and Applications.* HVAC&R research, 2007. **13**(6): p. 887-905.
8. Teshome, E.J. and F. Haghighat, *Zonal Models for Indoor Air Flow: A Critical Review.* International Journal of Ventilation, 2004. **3**(2): p. 119-129.
9. Megri, A.C., M. Snyder, and M. Musy, *Building Zonal Thermal and Airflow Modeling: A Review.* International Journal of Ventilation, 2005. **4**(2): p. 177-188.
10. Haghighat, F., Y. Li, and A.C. Megri, *Development and validation of a zonal model — POMA.* Building and Environment, 2001. **36**(9): p. 1039-1047.
11. Megri, A.C. and Y. Yu, *New calibrated zonal model (POMA+) for temperature and airflow predictions.* Building and Environment, 2015. **94**: p. 109-121.
12. Norrefeldt, V., G. Grün, and K. Sedlbauer, *VEPZO – Velocity propagating zonal model for the estimation of the airflow pattern and temperature distribution in a confined space.* Building and Environment, 2012. **48**: p. 183-194.
13. Wang, H. and Z. Zhai, *Application of coarse-grid computational fluid dynamics on indoor environment modeling: Optimizing the trade-off between grid resolution and simulation accuracy.* HVAC&R Research, 2012. **18**(5): p. 915-933.
14. Zuo, W. and Q. Chen, *Fast and informative flow simulations in a building by using fast fluid dynamics model on graphics processing unit.* Building and Environment, 2010. **45**(3): p. 747-757.
15. Jin, M., W. Liu, and Q. Chen, *Simulating buoyancy-driven airflow in buildings by coarse-grid fast fluid dynamics.* Building and Environment, 2015. **85**: p. 144-152.
16. Eriksson, L., et al. *CFD-free, efficient, micro indoor climate prediction in buildings*. in *BSO 2012 conference*. 2012. Loughborough.
17. Arai, Y., S. Togari, and K. Miura, *Unsteady-state thermal analysis of a large space with vertical temperature distribution.* ASHRAE Transactions, 1994. **100**(2): p. 396-411.
18. Togari, S., Y. Arai, and K. Miura, *Simplified model for predicting vertical temperature distribution in a large space.* ASHRAE Transactions, 1993. **99**(11): p. 84-99.
19. Takemasa, Y., S. Togari, and Y. Arai, *Application of an Unsteady-State Model for Predicting Vertical Temperature Distribution to an Existing Atrium.* ASHRAE Transactions, 1996. **102**(1): p. 239-247.
20. Gao, J., et al., *A heat transfer parameter at air interfaces in the BLOCK model for building thermal environment.* International Journal of Thermal Sciences, 2010. **49**(2): p. 463-470.
21. During, H., *Consommations énergétiques et confort thermiques des locaux chauffés: approche par les modèles zonaux*. 1994, INSA Lyon: Villeurbanne, France.
22. Musy, M., et al., *Generation of a zonal model to simulate natural convection in a room with a radiative/convective heater.* Building and Environment, 2001. **36**(5): p. 589-596.

23. Inard, C., P. Depecker, and J.J. Roux, *Un modèle simplifié pour la prédiction du champ de température dans les bâtiment.* Revue Générale de Thermique, 1997. **36**(113-123).
24. Georges, L., Ø. Skreiberg, and V. Novakovic, *On the proper integration of wood stoves in passive houses: investigation using detailed dynamic simulations.* Energy and Buildings, 2013. **59**: p. 203-213.
25. Georges, L., Ø. Skreiberg, and V. Novakovic, *On the proper integration of wood stoves in passive houses under cold climates.* Energy and Buildings, 2014. **72**: p. 87-95.
26. Georges, L. and Ø. Skreiberg, *Simple modelling procedure for the indoor thermal environment of highly insulated buildings heated by wood stoves.* Journal of Building Performance Simulation, 2016. **9**(6): p. 663-679.
27. CEN, *EN ISO 7730 : Ergonomics of the thermal environment: analytical determination and interpretation of thermal comfort using calculation of the PMV and PPD indices and local comfort criteria*. 2005, European Committee for Standardization.
28. Wang, H., et al., *On the calculation of heat migration in thermally stratified environment of large space building with sidewall nozzle air-supply.* Building and Environment, 2019. **147**: p. 221-230.
29. Morton, B.R., G. Taylor, and J.S. Turner, *Turbulent gravitational convection from maintained and instantaneous sources.* Proceedings of the Royal Society, 1956. **234**: p. 1-23.
30. Etheridge, D. and M. Sandberg, *Building ventilation: theory and measurements*. 1996, New Jersey: John Wiley and Sons.
31. Carlotti, P. and G.R. Hunt, *An entrainment model for lazy turbulent plumes.* Journal of Fluid Mechanics, 2017. **811**: p. 682-700.
32. Hunt, G.R. and N.B. Kaye, *Lazy plumes.* Journal of Fluid Mechanics, 2005. **533**: p. 329-338.
33. Thalfeldt, M., L. Georges, and Ø. Skreiberg. *Characterization of the free plume created by stove using laboratory measurements*. in *Roomvent & Ventilation 2018*. 2018. Helsinki, Finland.
34. Goodfellow, H.D., *Industrial ventilation design guidebook*. 2001: Elsevier.
35. Sahlin, P., et al., *Whole-building simulation with symbolic DAE equations and general purpose solvers.* Building and Environment, 2004. **39**: p. 949 – 958.
36. Dobrowolski, L., B. Giacomet, and N. Mendes. *Numerical Method for Calculating View Factor between Two Surfaces*. in *Building Simulation 2007*. 2007. Beijing, China.
37. Incropera, F., et al., *Fundamental of heat and mass transfer*. 6th ed. 2007, New Jersey: John Wiley and Sons.
38. Churchill, S. and H. Chu, *Correlating equations for laminar and turbulent free convection from a vectical plate.* International Journal of Heat and Mass Transfer, 1975. **18**: p. 1323-1329.
39. Johra, H. and P. Heiselberg, *Influence of internal thermal mass on the indoor thermal dynamics and integration of phase change materials in furniture for building energy storage: a review.* Renewable and Sustainable Energy Reviews, 2017. **69**: p. 19-32.
40. Reynders, G., *Quantifying the impact of building design on the potential of structural storage for active demand response in residential buildings*, in *Faculty of Engineering Science*. 2015, KU Leuven.